Rauwolfia serpentina Phytochemicals as Orexin Receptor-2 Agonists for Narcolepsy Management

Abstract

The neuropeptide orexin/hypocretin plays a crucial role in numerous physiological processes such as regulation of sleep/wakefulness, appetite and emotions. Dysregulation of orexin signaling has been implicated in hypersomnia, especially in narcolepsy, which is a chronic neurological disorder characterized by excessive daytime sleepiness (EDS), sudden loss of muscle tone while awake (cataplexy), sleep paralysis, and hallucinations. It is reported that lack of orexins contributes to the development of narcolepsy, thus small-molecule orexin receptor agonists have emerged as promising therapeutics for narcolepsy, and significant progress has been made in this domain in the past years. In the present study, we employed several bioinformatics tools to identify phytochemicals in *Rauvolfia serpentina* that may act as Orexin 2 receptor (OX2R) agonists. *In silico* approaches such as protein–ligand interaction analysis, drug–likeness evaluation, ADMET analysis, molecular docking, molecular dynamics simulation, and biological activity prediction, have been employed extensively. Among all the phytochemicals from *R. serpentina* that were virtually screened, tetraphylline and yohimbine were identified as promising drug candidates due to their favorable ADMET profile, high docking scores, permeability of the blood–brain barrier, and significant RMSD, RMSF, Rg, and SASA values. However, the study is solely based on *in silico* approaches, therefore *in vitro* and *in vivo* experimental studies are suggested to validate the potency and efficacy of these medications.

Keywords: orexin, narcolepsy, rauwolfia, MD simulation, in silico

Introduction

Narcolepsy is a rare neurological sleep disease that impairs the brain's capacity to control sleep–wake cycles, which hampers daily routines (Chavda et al., 2022; Chin et al., 2022). Individuals with narcolepsy experience drowsiness and daytime tiredness and may fall asleep quickly, which is known as a sleep attack (Schokman et al., 2024;). This sleep condition is defined as either

narcolepsy type 1 (NT1) which is characterized by symptoms of cataplexy and abrupt episodes of muscle weakness caused by emotion. Other type is narcolepsy type 2 (NT2) characterized by narcolepsy without cataplexy (Pizza et al., 2020; Alam et al., 2024). Cataplexy is characterized by the loss of muscular tone in awake conditions, resulting in weakness and loss of voluntary muscle control (Golden and Lipford, 2018). Cataplexy symptoms might emerge within weeks, months, or even years after the onset of excessive daily sleepiness (EDS). Few individuals may experience narcolepsy attack once or twice in their lifetime, whereas others may experience numerous attacks in a single day (Latorre et al., 2022). People with narcolepsy without cataplexy have excessive daytime sleepiness but do not typically suffer from muscle paralysis caused by emotions (Evans et al., 2022). NT1 is caused by degeneration of orexinergic neurons leading to decline in orexin level, which is a neuropeptide in the brain. Despite the ambiguity regarding the actual cause of NT2, certain cases have been linked to the diminished orexinergic neurons (Andlauer et al., 2012). Orexins (also called hypocretins) are neuropeptides that control arousal, alertness (Nevárez and Lecea 2018) and appetite (Liu et al., 2019). Orexins are found in two molecular forms. Their synthesis occurs in the hypothalamus by chemical cleavage of a 130 amino acid polypeptide called prepro-orexin (Abdel-Magid 2022). The first type, orexin A (OX-A) also known as hypocretin-1 is a 33-amino acid peptide consisting of two intramolecular disulfide bridges and the second is orexin B (OX-B) which is also known as hypocretin-2, is a linear 28-amino acid polypeptide (Soya and Sakurai 2020). The two known orexin receptors belong to the superfamily of G protein-coupled receptors (GPCRs) (Hellmann et al., 2020). Orexin-producing neurons (orexin neurons) spreads out axons throughout the brain. Interestingly, abundant population of orexinergic neurons are detected in the serotonergic dorsal raphe nucleus (DR), noradrenergic locus coeruleus (LC), and histaminergic tuberomammillary nucleus (TMN). They all are implicated in increasing arousal (Inutsuka and Yamanaka 2013). Various orexin knockout mice models exhibited significantly disrupted sleep–wake cycles (Thannickal et al., 2000; Mochizuki et al., 2004). Consistently, deficits in orexin function have been reported in human narcolepsy; these findings highlight the relevance of the orexin system in sleep/wake control (Peyron et al., 2000). The OX2R-specific agonist danavorexton (TAK-925, [methyl (2R,3S)-3-[(methylsulfonyl)amino]-2-{(cis-4-phenylcyclohexyl)oxy]piperidine-1-carboxylate]) was designed to address the lack of orexin signaling in NT1 and has shown >5,000-fold selectivity for human OX2R over OX1R in vitro (Yukitake et al., 2019). As orexin

neuropeptides cannot cross the blood–brain barrier (BBB), nonpeptide brain-penetrant orexin agonists are feasible treatment options for treating this sleeping disorder called narcolepsy (Fujiki et al., 2003).

Rauwolfia serpentina, also known as "Sarpagandha" in India, is a member of the Apocynaceae family (Paul et al., 2022). The Gangetic Plains, Eastern and Western Ghats, sub-Himalayan tracts, some areas of central India, and the Andaman Islands are among the places where it is most prevalent (Kumar et al., 2022). Owing to its therapeutic potential, *R. serpentine* is an important medicinal plant in the pharmaceutical sector (Sofowora et al., 2013). *R. serpentina* possess many phytochemical compounds, including flavonoids, alkaloids, tannins, and phenols, that have shown significant biological activity (Vaou et al., 2021; Abbas et al., 2024). Flavonoids obtained from this plant facilitate in various therapeutic applications and are being utilized in drug development (Roy et al., 2022). *R. serpentina* contain the alkaloid reserpine, which is a very useful agent for treating neurological diseases (Shah et al., 2020). This study aims to explore in silico and identify potent phytochemicals present in *R. serpentina* for their therapeutic effects on narcolepsy. The DISPEL (Diseases Plants Eliminate; https://compbio.iitr.ac.in/dispel/) server yielded *R. serpentina* as suitable plant source for phytochemicals for treatment of narcolepsy (Singh et al., 2023; Alam et al., 2024). Various computational approaches, such as molecular docking, molecular dynamic simulations, ADME/T analysis and physiochemical property determination, are taken into consideration. These parameters highlight the therapeutic potential of phytochemicals for narcolepsy treatment.

2. Materials and methods

2.1 Prediction of appropriate plant species

The Disease Plants Eliminate Sever (DISPEL) was used to project eligible plant species whose phytochemicals could serve as effective OX2R agonists (Singh et al., 2023). This platform serves as a comprehensive database with over 60,000 linkages between medicinal plants and disorders, representing approximately 5,500 species and 1,000 diseases globally. The DISPEL aid in variety of factors, including examining specific plants or diseases and conducting comparative studies on different plants and diseases (Alam et al., 2024). The website includes interactive visualizations such as network graphs, which make it easier to grasp the relationships between

therapeutic plants and diseases. The DISPEL server's search query "sleeping disorder" produced *R. serpentina* as the hit plant species (Figure 1).

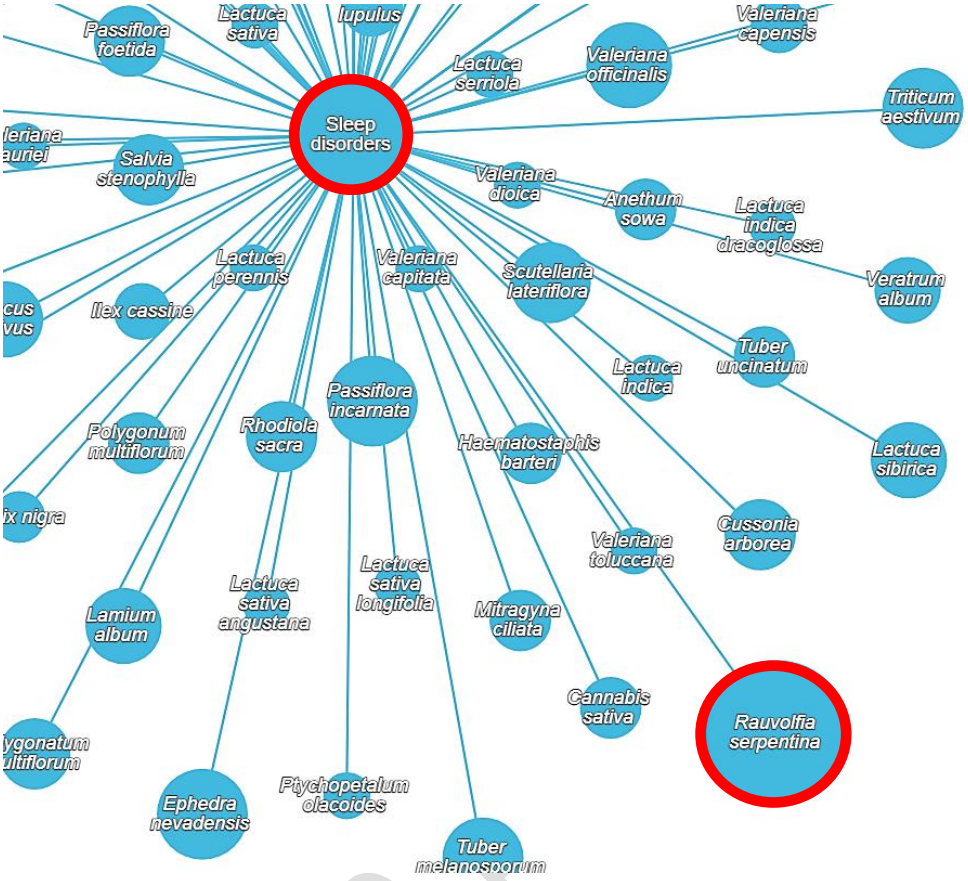

Figure 1: Interactive visualization of hit plant species for query search for sleep disorders via the DISPEL server

2.2 Assessment of phytochemicals in *Rauwolfia serpentina*

The phytochemicals in *R. serpentina* were analyzed via the Indian Medicinal Plants, Phytochemistry, and Therapeutics 2.0 (IMPPAT 2.0) platform (Vivek-Ananth et al., 2023). This collection has been meticulously reviewed, drawing on 100 traditional Indian medicine texts and over 7,000 published research publications, among additional reliable sources. IMPPAT 2.0 is the most complete compendium of phytochemical information from Indian medicinal plants to date, outperforming its predecessor, IMPPAT 1.0, with significant improvements and expansions.

2.3 Retrieval and preparation of target proteins

The three-dimensional crystal structure of OX2R was retrieved from the Protein Data Bank (PDB) with accession ID 7XRR. The protein structure for docking was prepared via UCSF Chimera 1.15 (Pettersen et al., 2004; Alam et al., 2023). Heteroatoms and water molecules were removed, and the Dockprep function of Chimera was employed for its preparation. Polar hydrogen atoms and Gasteiger charges were added, and the AMBERff14SB force field was applied.

2.4 Retrieval and preparation of ligands

The SDF files for the phytochemicals found in *R. serpentina* as assessed by IMPPAT 2.0 were retrieved from the PubChem database. Energy minimization of the ligands was performed via UCSF Chimera 1.15 software. The energy energy minimization parameters, such as the steepest descent steps, were set to 100, and a step size of 0.02 angstroms was used. The conjugate gradient steps were set to 10, with a step size of 0.02 angstroms. The phytochemicals retrieved from PubChem are listed in **Table 1** and their corresponding PubChem ID and molecular weight is mentioned.

Table 1: Details of phytochemicals from *R. serpentina* that are used for molecular docking with their PubChem ID and molecular weight

Ligand	**ID**	**Molecular weight (gram/mol)**
3-Oxorhazinilam	15173236	306.4
Papaverine	4680	339.4
Secologanin	161276	388.4
Tryptamine	1150	160.22
Raumacline	11723922	326.4
Serpentinine	5351576	685.8
Tetraphylline	164617	382.5
Vallesiachotamine	5384527	350.4
Reserpiline	67228	412.5
Rescinnamine	5280954	634.7
Macrophylline	5281737	239.31
Sarpagine	44592554	310.4

Raucaffrinoline	56927714	352.4
Vinburnine	71203	294.4
Rhazinilam	11312435	294.4
Deserpidine	8550	587.7
Isorauhimbine	6452110	354.4
Yohimbine	8969	354.4
Corynanthine	92766	354.4
Reserpine	5770	608.7

2.5 Virtual screening of phytochemicals against target proteins

The phytochemicals were screened virtually via AutoDock Vina 1.2.0 (Trott and Olson 2010), which is an integrated tool with PyRx 0.8 (Dallakyan and Olson 2015). PyRx is a commonly used molecular docking tool in the field of drug discovery that aids in virtual screening and evaluation of libraries of compounds against druggable targets.

2.6 Blood permeability assessment

Effective binding of a ligand with the OX2R receptor requires the ability to permeate the blood–brain barrier (BBB). The BBB permeability of the ligands was assessed via the BOILED-EGG feature of the SWISS ADME server (Daina and Zoete 2016).

2.7 ADMET analysis

The deep-PK webserver (Myung et al,. 2024) was used to analyze the ADMET properties of the selected phytochemicals. Deep-PK is a deep learning-based platform for predicting pharmacokinetics (PK) and toxicity, as well as for analysis and optimization. It utilizes graph neural networks approach and graph-based signatures to achieve optimal analytical performance across 73 endpoints, including 64 related to ADME/T and 9 general properties.

2.8 Biological activity prediction

Since OX2R is a G protein-coupled receptor (GPCR), phytochemicals must be capable of acting as GPCR ligands. The biological activity of the phytochemicals was evaluated via the

Molinspiration cheminformatics webserver (https://www.molinspiration.com) (Alam et al., 2024).

2.9 Drug-likeness properties of phytochemicals

Lipinski's rule of 5 was used to assess the drug-likeness of the phytochemicals. According to this rule, (1) the molecular mass should be under 500 Daltons to improve the absorption and distribution of the compound. (2) The LogP value indicates lipophilicity, which should be less than 5 to ensure adequate membrane permeability. (3) The compound should have no more than five hydrogen bond donors to enhance oral absorption. (4) It should have fewer than ten hydrogen bond acceptors to increase its solubility and bioavailability. (5) The molar refractivity value should be between 40 and 130 to ensure effective interaction with biological targets (Lipinski 2004). The evaluation was conducted via the Supercomputing Facility for Bioinformatics & Computational Biology (SCFBio) IIT Delhi server (http://www.scfbio-iitd.res.in/software/drugdesign/lipinski.jsp) (Jayaram et al., 2012).

2.10 Molecular dynamic simulation

Molecular dynamics (MD) simulation was performed with the complex of the OX2R receptor and selected phytochemicals via the WEBGRO macromolecular simulation server. This server is provided by the University of Arkansas for Medical Sciences (UAMS) through the GRACE High-Performance Computing Facility. Before these simulations were run, the molecular topologies of the compounds were created via the GlycoBioChemPRODRG2 server (http://davapc1.bioch.dundee.ac.uk/cgi-bin/prodrg) The simulations employed the GORMOS96 43A1 force field and used the SPC water model in a triclinic system with sodium chloride. Energy minimization of the resulting complexes was carried out via a steepest descent integrator, with steps taken every 5000 intervals. The system was then equilibrated under NVT/NPT conditions at 300 K and 1 bar pressure. The MD simulations were performed with a Leap-Frog integrator over 50 ns, which is constrained by available resources, and a total of 1000 frames were analyzed. The simulations included various parameters, such as the root-mean-square deviation (RMSD), root mean square fluctuation, radius of gyration (Rg), and solvent-accessible surface area (SASA). These parameters were used to examine the dynamics of the receptor–ligand complex (Bjelkmar et al., 2010; Lindorff-Larsen et al., 2010; Oostenbrink et al., 2004).

These findings help elucidate the interactions between the OX2R receptor and phytochemicals. Furthermore, the stability of the complexes was further assessed via normal mode analysis (NMA), which was performed via the iMOD server. iMOD enables vibrational analysis, motion animations, morphing trajectories, and Monte Carlo simulations via the "HA" coarse-graining model. Parameters such as eigenvalues, variance, and covariance maps were considered in the analysis (Lopéz-Blanco et al., 2011; Alam et al., 2024).

2.11 Visualization of interactions between phytochemicals and target proteins

The interaction between the ligands and the active site of the target protein was examined via LigPlot+ 2.2.8 (Laskowski and Swindells 2011), PyMOL 3.0 (Yuan et al., 2017), and Discovery Studio 2021 (Biovia, D.S. (2019) Discovery Studio Visualizer. San Diego). LigPlot+ software was used to generate two-dimensional plots to analyze hydrophobic and hydrogen bond interactions between the ligand and the protein. PyMOL and Discovery Studio were used to generate interactive 3D images of the protein–ligand interactions.

3. Results and discussion

3.1 Virtual screening of phytochemicals

The docking study was performed with the help of AutoDock Vina, which is integrated into PyRx 0.8. The phytochemicals were transformed to pdbqt format via Open Babel tool within PyRx. For docking, a grid box measuring 40.02 Å × 52.04 Å × 72.87 Å, centered at coordinates (-0.22, 5.56, 31.53), was used. The exhaustiveness level was set to value of 8 by default. Figure 2 shows the docking scores (kcal/mol) of the ligands. Docking scores provide details regarding the binding affinity of each ligand for the target protein. Typically, lower docking scores suggest stronger binding affinity and greater potential for drug effectiveness.

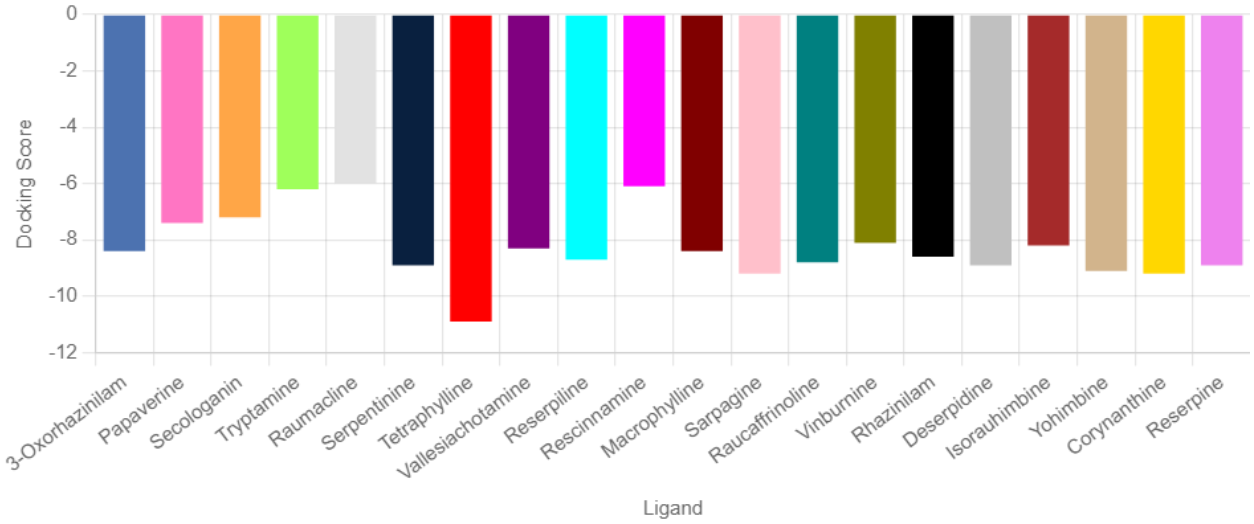

Figure 2: Docking scores of the phytochemicals in kcal/mol

2. Blood–brain barrier permeability

The BBB permeability of the phytochemicals was evaluated via the BOILED-EGG feature in the SWISS-ADME server. Phytochemicals in the yellow region of the BOILED-EGG can cross the BBB, whereas those outside this area do not possess this property. Figure 3 shows which phytochemicals have the potential to cross the BBB.

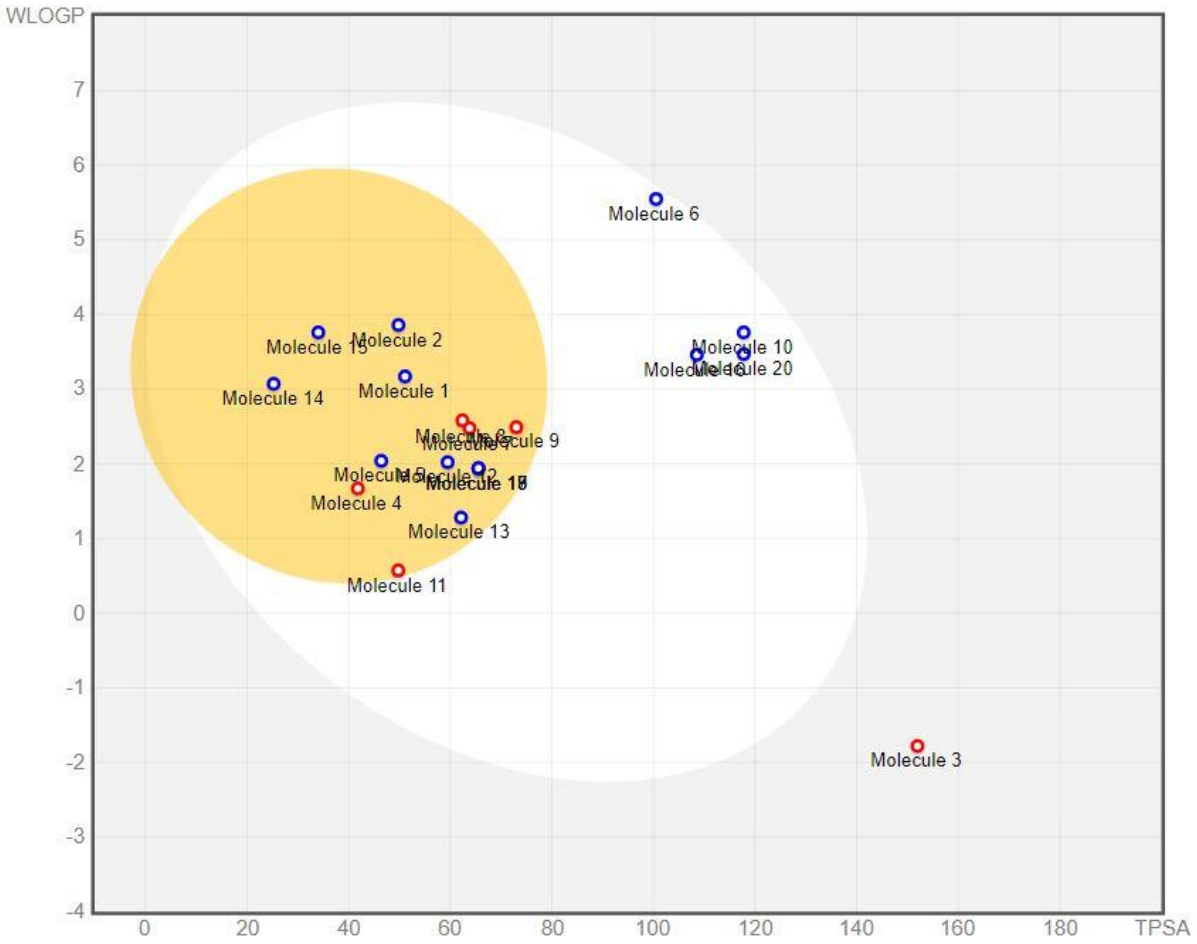

Figure 3: BOILED-EGG assessment for evaluating the ability of the ligands to permeate the BBB. Molecules that fall within the yellow (yolk) region are considered to have BBB permeant properties. The molecules with BBB-permeable properties are listed in **Table 2.**

Table 2: Phytochemicals with BBB-permeable properties along with their number of molecules, as shown in the BOILED-EGG diagram

Molecule number	**Ligand**
1	3-Oxorhazinilam
2	Papaverine
4	Tryptamine

5	Raumacline
7	Tetraphylline
8	Vallesiachotamine
9	Reserpiline
11	Macrophylline
12	Sarpagine
13	Raucaffrinoline
14	Vinburnine
15	Rhazinilam
17	Isorauhimbine
18	Yohimbine
19	Corynanthine

The top four phytochemicals with the highest blood–brain barrier permeability and the lowest docking scores were selected for further analysis.

2.3 Biological activity of selected phytocompounds

The biological activities of the selected compounds—tetraphylline, sarpagine, yohimbine, and corynanthine—were evaluated via the Molinspiration cheminformatics server. These compounds were analyzed for their potential as GPCR ligands. The activity scores were classified as follows: active (bioactivity score > 0), moderately active (bioactivity score between −5.0 and 0.0), and inactive (bioactivity score < −5.0). All four selected compounds were found to exhibit GPCR ligand properties, as indicated by their bioactivity scores, which were all greater than 0 (**Table 3**).

Table 3: Bioactivity score for being a GPCR ligand for the selected phytocompounds as per the Molinspiration webserver

Ligand	Bioactivity score
Tetraphylline	0.35
Sarpagine	0.72
Corynanthine	0.47
Yohimbine	0.47

2.4 ADMET analysis

ADMET analysis of the selected phytocompounds was performed via the Deep-PK server. The results of the analysis are detailed in Table 4. ADMET analysis of corynanthine indicated that it is bioavailable with a probability of 0.59 and has a high probability of human intestinal absorption of 0.969, which is interpreted as high absorption. It is not a P-glycoprotein (P-gp) inhibitor but acts as a P-gp substrate with a medium confidence probability of 0.703. Corynanthine can penetrate the BBB with high confidence. It binds to 57.25% of plasma proteins, which is within the therapeutic range. The metabolic profile shows that it is generally noninhibitory for various CYP enzymes except for CYP2D6, which it inhibits with high confidence. It also acts as a substrate for most CYP enzymes in addition to CYP2C19 and CYP2C9. The clearance of corynanthine is predicted to be 10.77, with a half-life of less than 3 hours, suggesting rapid elimination. Toxicity predictions show that it is safe in the context of mutagenesis, avian toxicity, bioconcentration, biodegradation, carcinogenesis, and liver injury. ADMET analysis of yohimbine suggested a bioavailability probability of 0.54 and a high intestinal absorption probability of 0.967. Yohimbine is not a P-gp inhibitor but is a substrate with medium confidence. It can cross the BBB with high confidence and bind to plasma proteins at 57.74% confidence. The metabolic profile revealed that it is noninhibitory to most CYP enzymes but inhibits CYP2D6. Yohimbine is also a substrate for multiple CYP enzymes, in

addition to CYP2C19 and CYP2C9. It has a clearance of 10.66 and a predicted half-life of less than 3 hours, indicating quick elimination. Toxicity analysis revealed that yohimbine is safe for mutagenesis, avian toxicity, bioconcentration, biodegradation, carcinogenesis, and liver injury. Tetraphylline is bioavailable with a probability of 0.682 and has a high probability of human intestinal absorption of 0.976. It acts as a P-gp inhibitor and substrate but with low confidence. Tetraphylline has the ability to penetrate the BBB with high confidence. It also binds to plasma proteins at 7.29%, indicating a low binding rate. In terms of metabolism, the tetraphylline is noninhibitory to most CYP enzymes, except for CYP2D6 and CYP3A4. It acts as a substrate for various CYP enzymes, excluding CYP2C9. Tetraphylline has a clearance of 11.36 and a predicted half-life of less than 3 hours, implying rapid clearance. Toxicity analysis revealed that it is safe for mutagenesis, avian toxicity, bioconcentration, biodegradation, carcinogenesis, and liver injury. Sarpagine has a bioavailability probability of 0.562 and a high probability of human intestinal absorption of 0.985. Sarpagine can cross the BBB with high confidence. It binds to plasma proteins at 58.42% identity. It is an inhibitor of CYP1A2 with medium confidence and inhibits CYP 2D6 with high confidence while being a substrate for most CYP enzymes except CYP 1A2 and CYP 2C9. The clearance of sarpagine is predicted to be 16.15, with a half-life of less than 3 hours, indicating that it is rapidly cleared. Toxicity predictions suggest that sarpagine is safe for mutagenesis, avian toxicity, bioconcentration, biodegradation, carcinogenesis, and liver injury.

The ADMET analysis of the selected compounds revealed that all the compounds presented favorable ADMET profiles, indicating their potency as drug candidates.

Table 4. ADMET profile of the selected phytocompounds according to the Deep-PK server

Parameter	Property	Corynanthine	Yohimbine	Tetraphylline	Sarpagine
	Human Oral Bioavailability Probability	0.59	0.54	0.682	0.562
	Human Oral Bioavailability Interpretation	Bioavailable	Bioavailable	Bioavailable	Bioavailable

Absorption	Human Intestinal Absorption Predictions	Absorbed	Absorbed	Absorbed	Absorbed
	Human Intestinal Absorption Probability	0.969	0.967	0.976	0.985
	Human Intestinal Absorption Interpretation	Absorbed (High Confidence)	Absorbed (High Confidence)	Absorbed (High Confidence)	Absorbed (High Confidence)
	Human Oral Bioavailability Predictions	Bioavailable	Bioavailable	Non-Bioavailable	Non-Bioavailable
	Human Oral Bioavailability Probability	0.566	0.596	0.414	0.437
	Human Oral Bioavailability Interpretation	Bioavailable	Bioavailable	Non-Bioavailable	Non-Bioavailable
	P-Glycoprotein Inhibitor Predictions	Non-Inhibitor	Non-Inhibitor	Inhibitor	Inhibitor
	P-Glycoprotein Inhibitor Probability	0.012	0.012	0.577	0.64
	P-Glycoprotein Inhibitor Interpretation	Non-Inhibitor (High Confidence)	Non-Inhibitor (High Confidence)	Inhibitor (Low Confidence)	Inhibitor (Low Confidence)

	P-Glycoprotein Substrate Predictions	Substrate	Substrate	Substrate	Substrate
	P-Glycoprotein Substrate Probability	0.703	0.707	0.569	0.628
	P-Glycoprotein Substrate Interpretation	Substrate (Medium Confidence)	Substrate (Medium Confidence)	Substrate (Low Confidence)	Substrate (Low Confidence)
Distribution	Blood–Brain Barrier Predictions	Penetrable	Penetrable	Penetrable	Penetrable
	Blood–Brain Barrier Probability	1	1	0.999	0.997
	Blood–Brain Barrier Interpretation	Penetrable (High Confidence)	Penetrable (High Confidence)	Penetrable (High Confidence)	Penetrable (High Confidence)
	Plasma Protein Binding Predictions	57.25%	57.74%	7.29%	58.42%
	Plasma Protein Binding Interpretation	Proper Value: therapeutic index < 90%; Poor Value value > 90%			
	CYP 1A2 Inhibitor Predictions	Non-Inhibitor	Non-Inhibitor	Non-Inhibitor	Inhibitor
	CYP 1A2 Inhibitor Probability	0.161	0.208	0.275	0.695
	CYP 1A2	Non-Inhibitor	Non-	Non-Inhibitor	Inhibitor

	Inhibitor Interpretation	(High Confidence)	Inhibitor (Medium Confidence)	(Medium Confidence)	(Medium Confidence)
	CYP 1A2_substrate Predictions	Substrate	Substrate	Substrate	Non-Substrate
	CYP 1A2_substrate Probability	0.554	0.557	0.762	0.399
	CYP 1A2_substrate Interpretation	Substrate (Low Confidence)	Substrate (Low Confidence)	Substrate (Medium Confidence)	Non-Substrate (Low Confidence)
Metabolism	CYP 2C19 Inhibitor Predictions	Non-Inhibitor	Non-Inhibitor	Non-Inhibitor	Non-Inhibitor
	CYP 2C19 Inhibitor Probability	0.228	0.283	0.031	0.019
	CYP 2C19 Inhibitor Interpretation	Non-Inhibitor (Medium Confidence)	Non-Inhibitor (Medium Confidence)	Non-Inhibitor (High Confidence)	Non-Inhibitor (High Confidence)
	CYP 2C19_substrate Predictions	Non-Substrate	Non-Substrate	Substrate	Substrate
	CYP 2C19_substrate Probability	0.466	0.468	0.577	0.537
	CYP 2C19_substrate	Non-Substrate	Non-Substrate	Substrate (Low	Substrate (Low

	Interpretation	(Low Confidence)	(Low Confidence)	Confidence)	Confidence)
	CYP 2C9 Inhibitor Predictions	Non-Inhibitor	Non-Inhibitor	Non-Inhibitor	Non-Inhibitor
	CYP 2C9 Inhibitor Probability	0.006	0.004	0.017	0.03
	CYP 2C9 Inhibitor Interpretation	Non-Inhibitor (High Confidence)	Non-Inhibitor (High Confidence)	Non-Inhibitor (High Confidence)	Non-Inhibitor (High Confidence)
	CYP 2C9 Substrate Predictions	Non-Substrate	Non-Substrate	Non-Substrate	Non-Substrate
	CYP 2C9 Substrate Probability	0.281	0.279	0.375	0.014
	CYP 2C9 Substrate Interpretation	Non-Substrate (Medium Confidence)	Non-Substrate (Medium Confidence)	Non-Substrate (Low Confidence)	Non-Substrate (High Confidence)
	CYP 2D6 Inhibitor Predictions	Inhibitor	Inhibitor	Inhibitor	Inhibitor
	CYP 2D6 Inhibitor Probability	0.998	0.998	0.947	0.999
	CYP 2D6 Inhibitor Interpretation	Inhibitor (High Confidence)	Inhibitor (High Confidence)	Inhibitor (High Confidence)	Inhibitor (High Confidence)

	CYP 2D6 Substrate Predictions	Substrate	Substrate	Substrate	Substrate
	CYP 2D6 Substrate Probability	0.518	0.518	0.505	0.658
	CYP 2D6 Substrate Interpretation	Substrate (Low Confidence)	Substrate (Low Confidence)	Substrate (Low Confidence)	Substrate (Low Confidence)
	CYP 3A4 Inhibitor Predictions	Non-Inhibitor	Non-Inhibitor	Inhibitor	Non-Inhibitor
	CYP 3A4 Inhibitor Probability	0.117	0.092	0.596	0.007
	CYP 3A4 Inhibitor Interpretation	Non-Inhibitor (High Confidence)	Non-Inhibitor (High Confidence)	Inhibitor (Low Confidence)	Non-Inhibitor (High Confidence)
	CYP 3A4 Substrate Predictions	Substrate	Substrate	Substrate	Substrate
	CYP 3A4 Substrate Probability	0.903	0.903	0.823	0.737
	CYP 3A4 Substrate Interpretation	Substrate (High Confidence)	Substrate (High Confidence)	Substrate (Medium Confidence)	Substrate (Medium Confidence)
	Clearance Predictions	10.77	10.66	11.36	16.15
	Half-Life of	Half-Life <	Half-Life <	Half-Life <	Half-Life <

Excretion	Drug Predictions	3hs	3hs	3hs	3hs
	Half-Life of Drug Probability	0.109	0.103	0.143	0.134
	Half-Life of Drug Interpretation	Half-Life < 3hs (High Confidence)	Half-Life < 3hs (High Confidence)	Half-Life < 3hs (High Confidence)	Half-Life < 3hs (High Confidence)
Toxicity	AMES Mutagenesis Predictions	Safe	Safe	Safe	Safe
	Avian Predictions	Safe	Safe	Safe	Safe
	Bioconcentration Factor Predictions	0.45	0.5	0.73	-0.41
	Bioconcentration Factor Interpretation	None	None	None	None
	Biodegradation Predictions	Safe	Safe	Safe	Safe
	Biodegradation Probability	0.001	0.001	0.002	0
	Biodegradation Interpretation	Safe (High Confidence)	Safe (High Confidence)	Safe (High Confidence)	Safe (High Confidence)
	Carcinogenesis Predictions	Safe	Safe	Safe	Safe
	Carcinogenesis Probability	0.324	0.321	0.161	0.069
	Carcinogenesis Interpretation	Safe (Medium Confidence)	Safe (Medium Confidence)	Safe (High Confidence)	Safe (High Confidence)

	Liver Injury I Predictions	Safe	Safe	Safe	Safe
	Liver Injury I Probability	0.296	0.284	0.405	0.296
	Liver Injury I Interpretation	Safe (Medium Confidence)	Safe (Medium Confidence)	Safe (Low Confidence)	Safe (Medium Confidence)

2.5 Drug-likeness property assessment

The drug-likeness properties of the selected phytocompounds were analyzed via the SCFBio server, with Lipinski's rule of 5 used as a standard. According to this rule, (1) the molecular mass should be under 500 Daltons to improve the absorption and distribution of the compound. (2) The LogP value indicates lipophilicity, which should be less than 5 to ensure adequate membrane permeability. (3) The compound should have no more than five hydrogen bond donors to enhance oral absorption. (4) It should have fewer than ten hydrogen bond acceptors to increase its solubility and bioavailability. (5) The molar refractivity value should be between 40 and 130 to ensure effective interaction with biological targets. All the selected phytochemicals follow the Lipinski rule of five, indicating their drug-likeness (**Figure 4 (a-e)**).

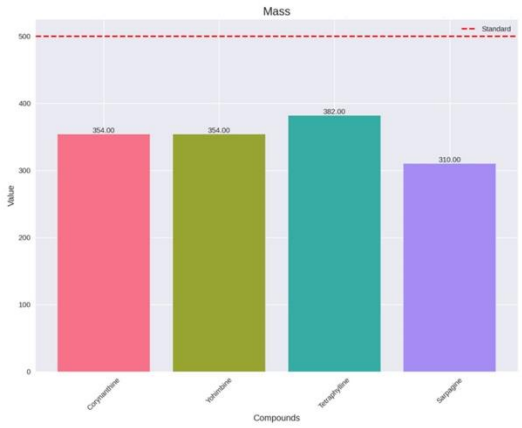
Mass
Standard
500
400
300
200
100
0
Value
354.00
354.00
382.00
310.00
Corynanthine
Yohimbine
Tetraphylline
Sarpagine
Compounds

(a)

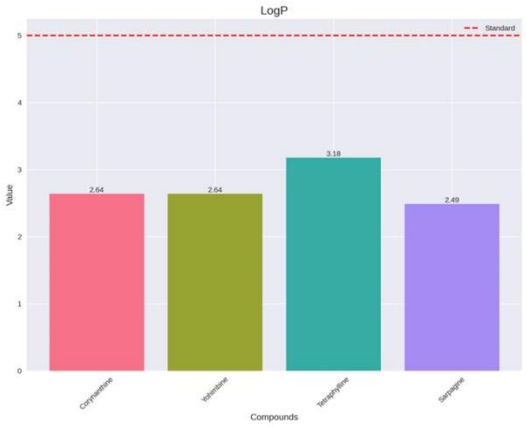
LogP
Standard
5
4
3
2
1
0
Value
2.64
2.64
3.18
2.49
Corynanthine
Yohimbine
Tetraphylline
Sarpagine
Compounds

(b)

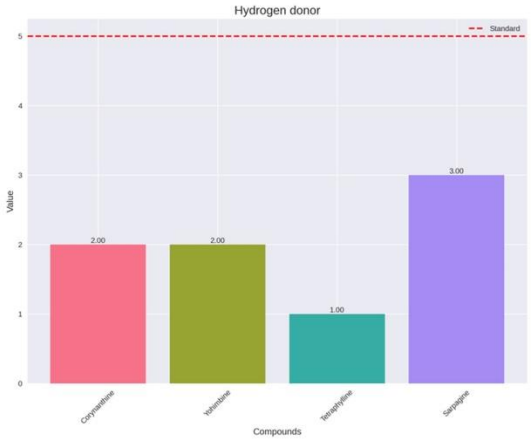
Hydrogen donor
Standard
5
4
3
2
1
0
Value
2.00
2.00
1.00
3.00
Corynanthine
Yohimbine
Tetraphylline
Sarpagine
Compounds

(c)

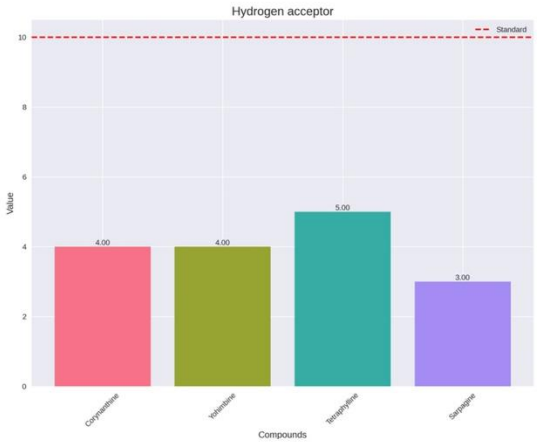
Hydrogen acceptor
Standard
10
8
6
4
2
0
Value
4.00
4.00
5.00
3.00
Corynanthine
Yohimbine
Tetraphylline
Sarpagine
Compounds

(d)

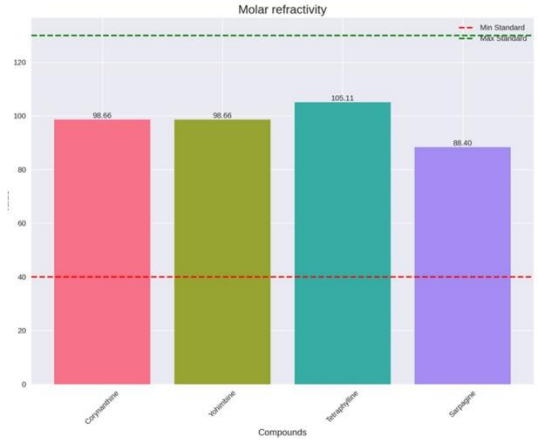
Molar refractivity
Min Standard
120
100
80
60
40
20
0
98.66
98.66
105.11
88.40
Corynanthine
Yohimbine
Tetraphylline
Sarpagine
Compounds

(e)

Figure 4a-e. Observed values for the parameters of the Lipinski rule of five: (a) molecular mass, (b) LogP (lipophilicity), (c) hydrogen donor, (d) hydrogen acceptor, and (e) molar refractivity

2.6 Molecular dynamic simulation

Present investigation explores in depth receptor–ligand complexes via MD simulation study. The primary goal was to elucidate pivotal constraints such as the RMSD, RMSF, SASA, and Rg. MD simulations spanning over 50 ns provide crucial understandings regarding dynamic interactions between the receptor and the ligands. The RMSD trajectories derived from these simulations were consistent with the data obtained from docking studies. These trajectories offer a time-based view of the contact between the ligand and the receptor during the 50 ns simulation period. The RMSD values are indicative of the stability of the protein–ligand complex.

Figure 5 illustrates the RMSD analysis for the interactions of corynanthine, sarpagine, tetraphylline, and yohimbine with the OX2R receptor binding site. The corynanthine complex revealed significant variations, which indicates structural instability. In contrast, the tetraphylline complex presented the lowest RMSD value and the least fluctuation, indicating greater structural stability. Yohimbine showed rapid RMSD fluctuations at the initial stages of the simulation but later stabilized.

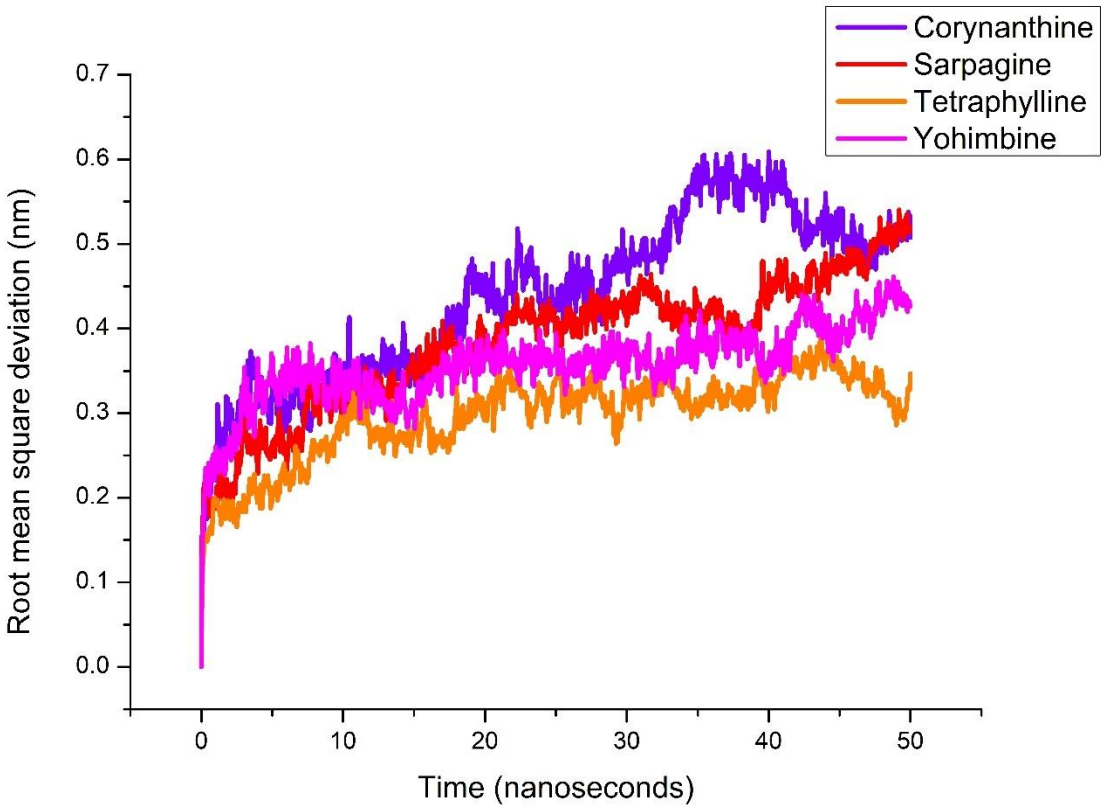

Figure 5. Root mean square deviation (RMSD) graph for complexes: (a) corynanthine (purple), (b) sarpagine (red), (c) tetraphylline (orange), and (d) yohimbine (magenta)

The RMSF is an important measure for assessing the conformational stability of macromolecular structures. The RMSF demonstrates the flexibility of individual residues by calculating the mean square root of atomic position variations. Reduced coordinate fluctuations suggest increased stability. Furthermore, symmetrical fluctuations imply more homogeneous stability than asymmetrical variances. The RMSF values emphasize that variations within specific areas provide insight into ligand-induced conformational changes. The RMSF of the protein–ligand complexes exhibited symmetrical variations, indicating that the combination remained stable throughout the simulation period (Figure 6). This stability shows that the phytocompounds have agonistic characteristics, which indicate their potential as receptor ligands.

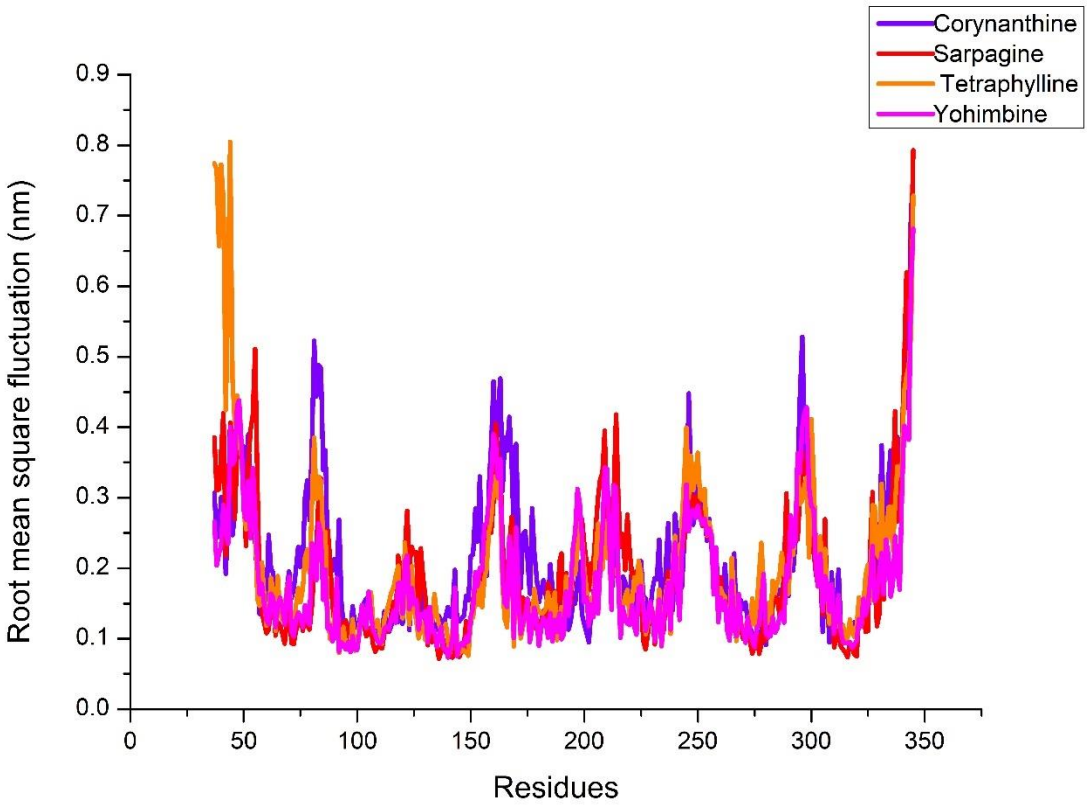

Figure 6. Root mean square fluctuation (RMSF) graph for complexes: (a) corynanthine (purple), (b) sarpagine (red), (c) tetraphylline (orange), and (d) yohimbine (magenta)

The firmness of OX2R structure in the presence of certain ligands was assessed via the use of Rg. Rg offers insight into the three-dimensional positioning of the secondary structure of a protein. In this context, compactness is defined as the ratio of the accessible surface area to the surface area of a perfect sphere with an equivalent volume. A reduced Rg denotes a more compact configuration of the protein. Thus, trajectory analysis makes it easier to investigate how variations in the compactness of OX2R are influenced by the selected compounds. Notably, tetraphylline and yohimbine show the most significant compactness, as shown by their minimum Rg values (Figure 7).

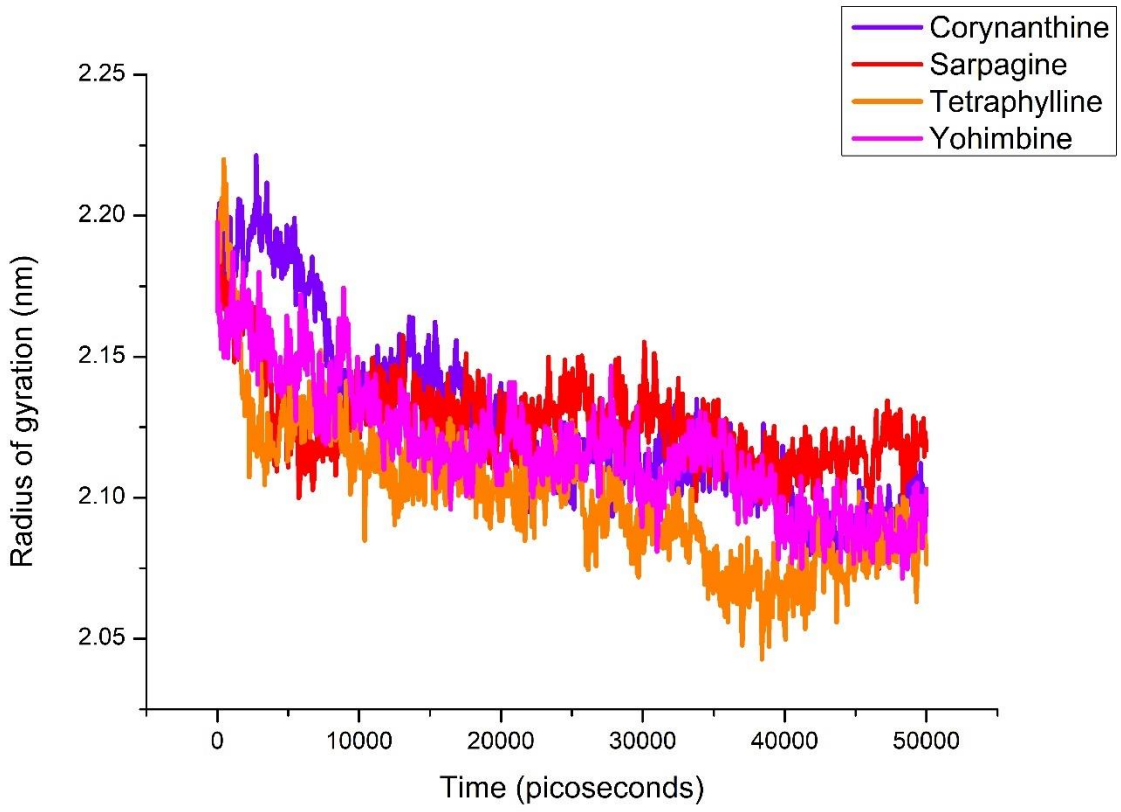

Figure 7. Radii of gyration of the complexes: (a) corynanthine (purple), (b) sarpagine (red), (c) tetraphylline (orange), and (d) yohimbine (magenta)

Changes in the surface area of the protein were determined by analyzing the SASA of the complexes. An increase in SASA values suggests an increase in surface area, whereas a decrease in SASA values suggests a decrease in protein volume. Protein structure compactness and SASA have an inverse connection, meaning that a lower SASA value corresponds to greater structural compactness. Tetraphylline, yohimbine, and sarpagine were found to have the lowest SASA values, as shown in Figure 8, suggesting the compactness and stability of the complexes.

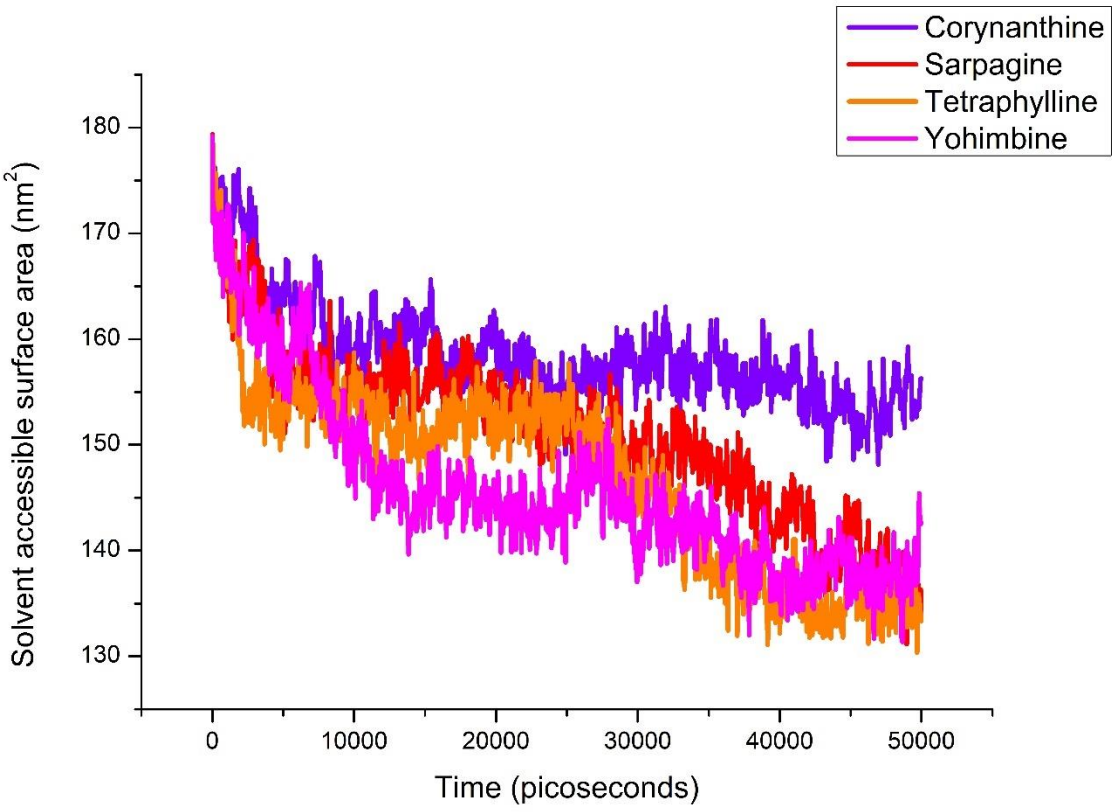

Figure 8. Solvent accessible surface areas of the complexes: (a) corynanthine (purple), (b) sarpagine (red), (c) tetraphylline (orange), and (d) yohimbine (magenta)

The complexes were further evaluated for NMA analysis via the iMOD server. This webserver provides several analytical metrics, such as complex deformability, B-factors, eigenvalues, variance, covariance maps, and elastic network data. The B factor aids in quantifying the atomic displacement or flexibility within the protein structure. Its high value indicates increased flexibility. A comparison between the NMA and Protein Data Bank (PDB) B-factors suggested that the normal modes accurately reflect the dynamic behavior of the protein. The deformability plot illustrates that the molecule can be deformed with ease, while peaks indicate areas of greater flexibility. These specified regions are critical for understanding the functional movements within the protein structure. The eigenvalue plot provides insight into the stiffness of the modes. Lower eigenvalues correspond to softer modes that are more susceptible to deformation. The variance graph depicts the cumulative variance explained by the modes. higher modes capturing more complex motions. This cumulative plot assists in determining the number of modes

necessary to account for a substantial portion of the protein's dynamic behavior. The elastic network model presents a grayscale map of pairwise interaction strengths between atoms, where darker regions denote stronger interactions. The highlighted regions suggest increased rigidity and contribute to maintaining the structural integrity of the target protein. Furthermore, the covariance map reveals correlated motions between residue pairs. The red regions signify high positive correlations where residues move together. The blue regions denote negative correlations, which indicate opposite movements. This information is crucial for understanding the collective motions within the protein and identifying key residues involved in these movements.

NMA results for the corynanthine (Figure 9A), sarpagine (Figure 9B), tetraphylline (Figure 9C), and yohimbine (Figure 9D) complexes with OX2R revealed insights into their structural dynamics and stability. All four structures exhibit identical patterns in their B factor plots, indicating regions of high flexibility, particularly toward the ends of their sequences. The deformability graphs for each complex emphasize certain areas that are more susceptible to undergo conformational changes. These areas might be crucial for the biological functions of the compound. The eigenvalue plots for all four complexes show a consistent increasing trend, with the first eigenvalues ranging from approximately 1.14e-03 to 1.22e-03. This similarity suggests that these compounds may require comparable energy inputs to undergo structural deformations, indicating their stability. The variance plots indicate that the initial modes capture a significant portion of the overall dynamic behavior for all the structures, which is typical for biological molecules. Comparison of the elastic network and covariance maps across the four structures revealed complex interaction networks and correlated movements for each molecule. However, the tetraphylline-OX2R complex seems to have a more complex pattern in its elastic network, which may be due to its larger size and complexity as a protein–ligand complex. Among these complexes, the tetraphylline-OX2R complex likely represents the most compact and stable structure. This assessment is based on its more complex elastic network, which suggests a greater degree of intramolecular interactions.

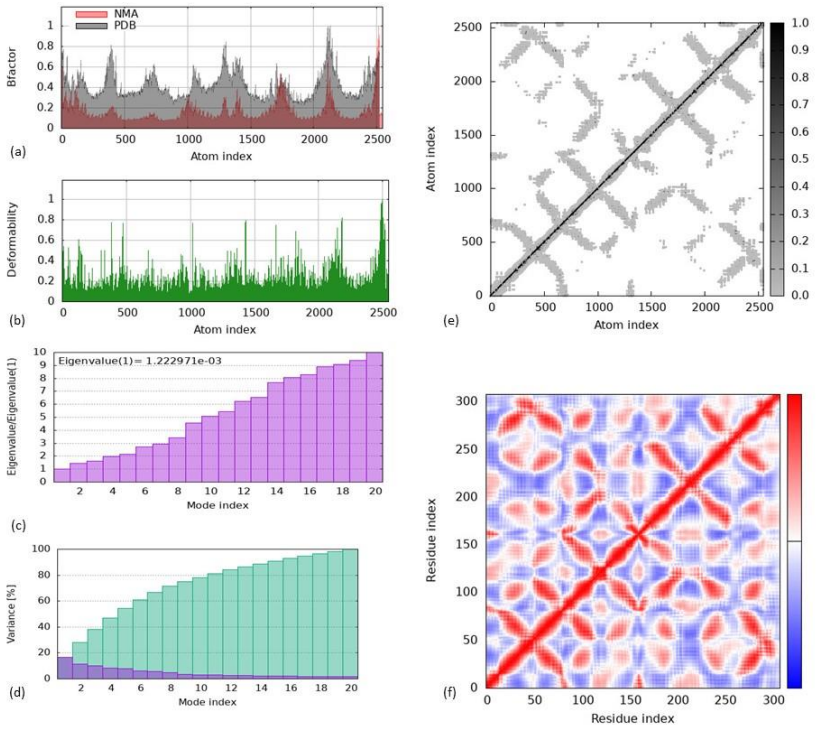
NMA
PDB
Bfactor
(a)
Atom index
Deformability
(b)
Atom index
Eigenvalue(1)= 1.222971e-03
Eigenvalue/Eigenvalue(1)
(c)
Mode index
Variance [%]
(d)
Mode index
Atom index
(e)
Atom index
Residue index
(f)
Residue index

(A)

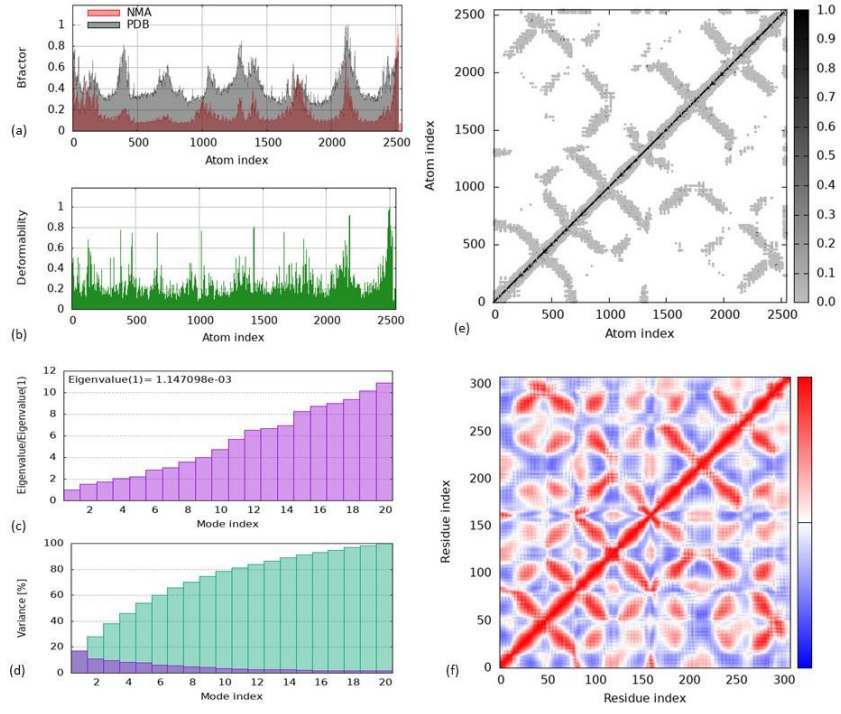
NMA
PDB
Bfactor
(a)
Atom index
Deformability
(b)
Atom index
Eigenvalue(1)= 1.147098e-03
Eigenvalue/Eigenvalue(1)
(c)
Mode index
Variance [%]
(d)
Mode index
Atom index
(e)
Atom index
Residue index
(f)
Residue index

(B)

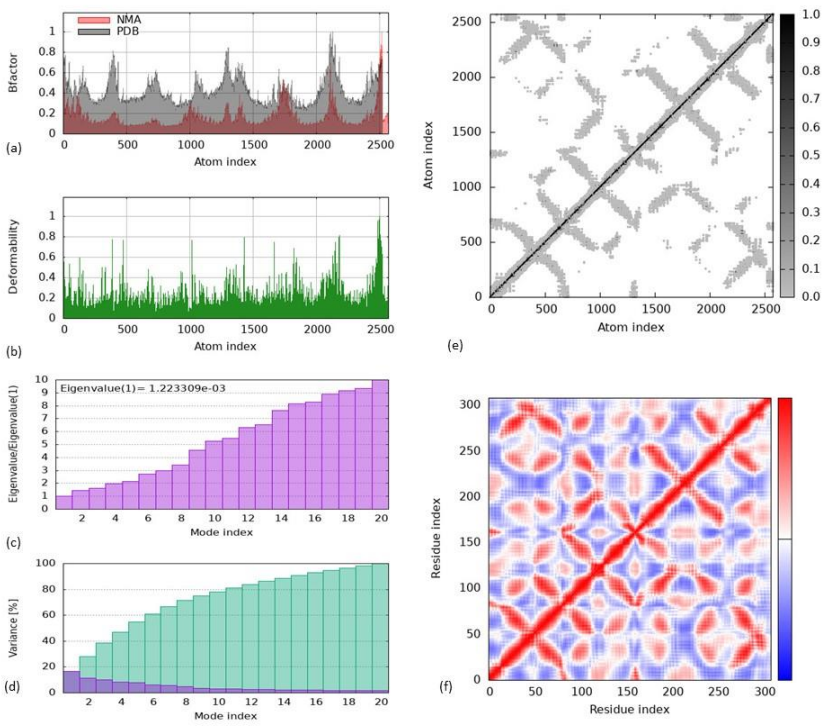
NMA
PDB
Bfactor
(a)
Atom index
Deformability
(b)
Atom index
Eigenvalue(1)= 1.223309e-03
Eigenvalue/Eigenvalue(1)
(c)
Mode index
Variance [%]
(d)
Mode index
Atom index
Atom index
(e)
Residue index
Residue index
(f)

(C)

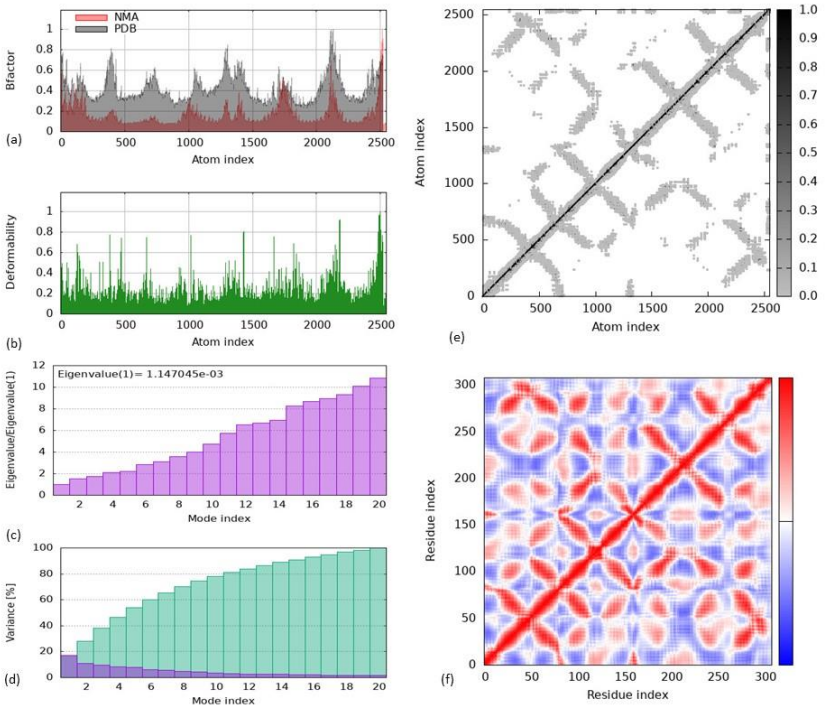
NMA
PDB
Bfactor
(a)
Atom index
Deformability
(b)
Atom index
Eigenvalue(1)= 1.147045e-03
Eigenvalue/Eigenvalue(1)
(c)
Mode index
Variance [%]
(d)
Mode index
Atom index
Atom index
(e)
Residue index
Residue index
(f)

(D)

Figure 9A-D. Interactive depiction of the NMA analysis results obtained from the iMOD server.

(a) B-factor plot, (b) Deformability plot, (c) Eigenvalues, (d) Variance, (e) elastic network model, (f) covariance

2.7 Interaction of phytocompounds with the target

The interaction of the ligands with the active site of the target protein is detailed in Table 5, while a 3D representation is given in Figure 10 a-d. Corynanthine interacts hydrophobically with the residues Tyr53, Glu54, Val56, Leu57, Tyr343, Ala344, Thr347, Phe348, and Trp351 of the target protein. It forms hydrogen bonds with the residues Lys51 and Glu340, with bond lengths of 3.20 Å and 2.83 Å, respectively. Yohimbine has hydrophobic interactions with the residues Thr111, Ile130, Pro131, Val138, Phe227, Ile320, Asp324, His350, and Ser321. Furthermore, it forms hydrogen bonds with the residues Gln134 and Tyr354, with bond lengths of 3.01 Å and 2.75 Å, respectively. Sarpagine is involved in hydrophobic interactions with the residues Ala110, Val114, Pro131, Gln134, Thr135, Phe227, Ile320, His350, and Val353. It forms hydrogen bonds with the residues Thr111 and Tyr354, with bond lengths of 2.75 Å and 3.09 Å, respectively. The tetraphylline shows hydrophobic interactions with the residues Val52, Tyr53, Val56, Leu57, Asp115, Tyr343, Ala344, Trp345, Thr347, and Phe348. It forms a hydrogen bond with the residue Lys51, with a bond length of 3.04 Å.

Table 5. Interactions between selected phytochemicals and the active site of the target protein

Ligand	Type of Interaction	Residues	Bond length (Å)
Corynanthine	Hydrophobic	Tyr53, Glu54, Val56, Leu57, Tyr343, Ala344, Thr347, Phe348, Trp351	----
	Hydrogen bond	Lys51 Glu340	3.20 2.83
Yohimbine	Hydrophobic	Thr111, Ile130, Pro131, Val138, Phe227, Ile320, Asp324, His350, Ser321	----
	Hydrogen bond	Gln134 Tyr354	3.01 2.75
Sarpagine	Hydrophobic	Ala110, Val114, Pro131, Gln134, Thr135, Phe227, Ile320, His350, Val353	----
	Hydrogen bond	Thr111 Tyr354	2.75 3.09
Tetraphylline	Hydrophobic	Val52, Tyr53, Val56, Leu57, Asp115, Tyr343, Ala344, Trp345, Thr347, Phe348	----

	Hydrogen bond	Lys51	3.04

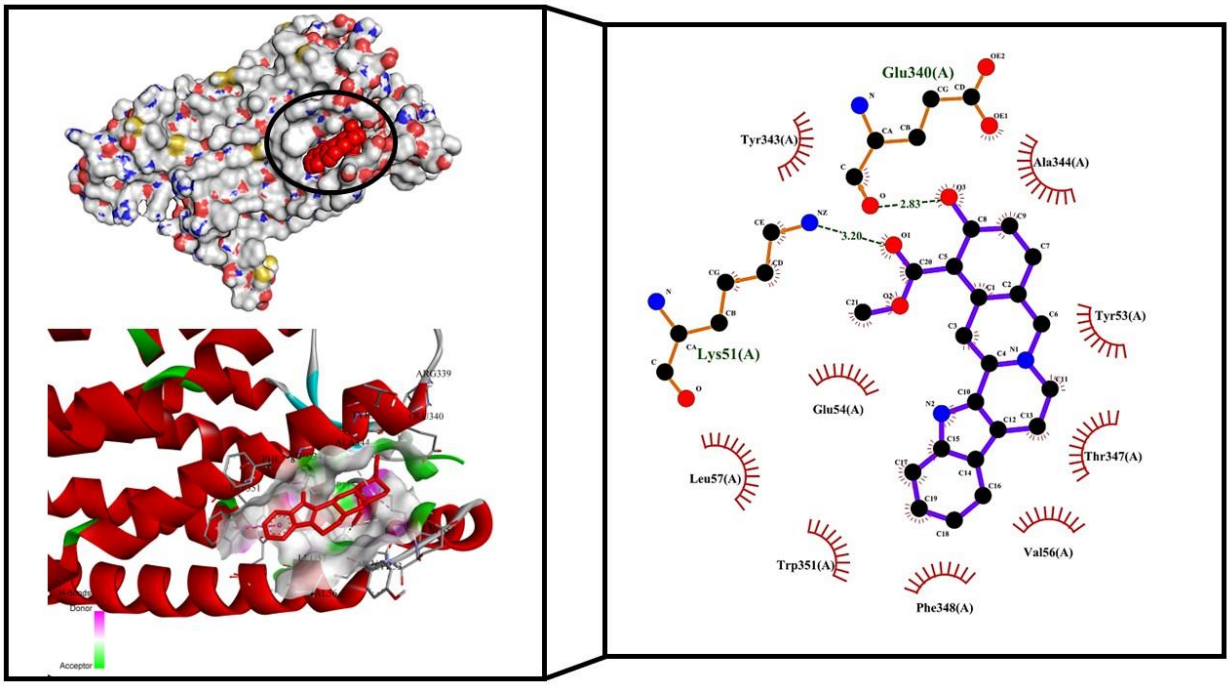

(a)

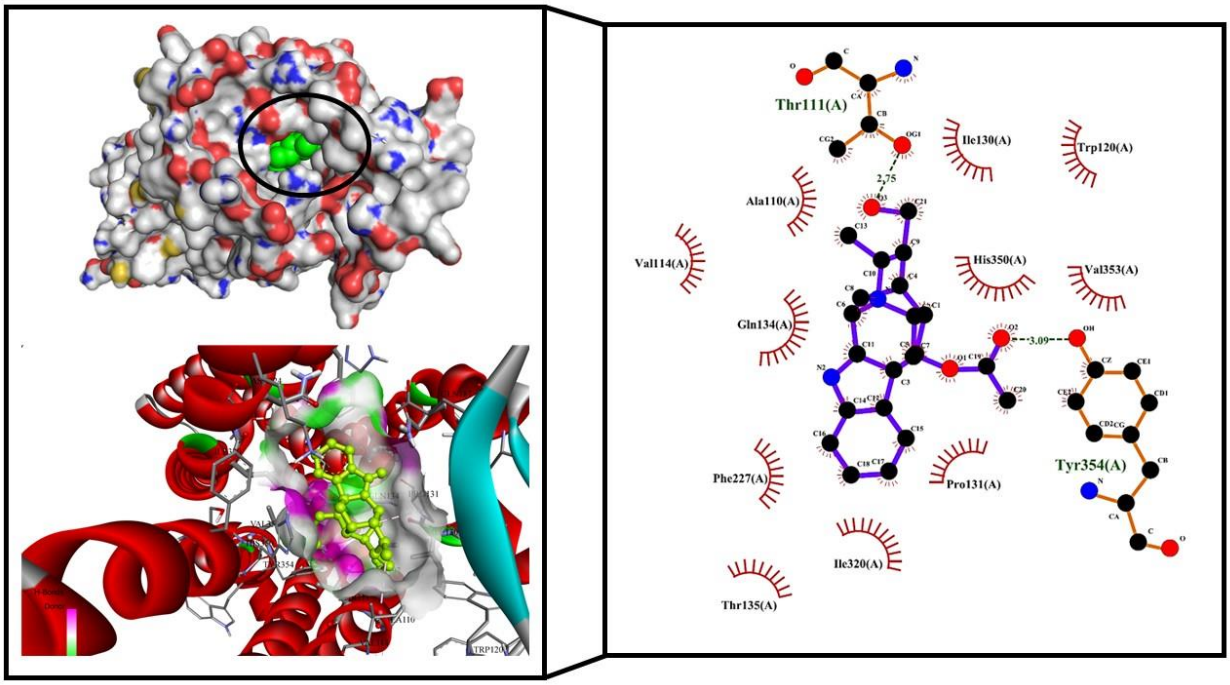
Thr111(A)
Ile130(A)
Trp120(A)
2.75
Ala110(A)
Val114(A)
His350(A)
Val353(A)
Gln134(A)
3.09
Tyr354(A)
Phe227(A)
Pro131(A)
Ile320(A)
Thr135(A)

(b)

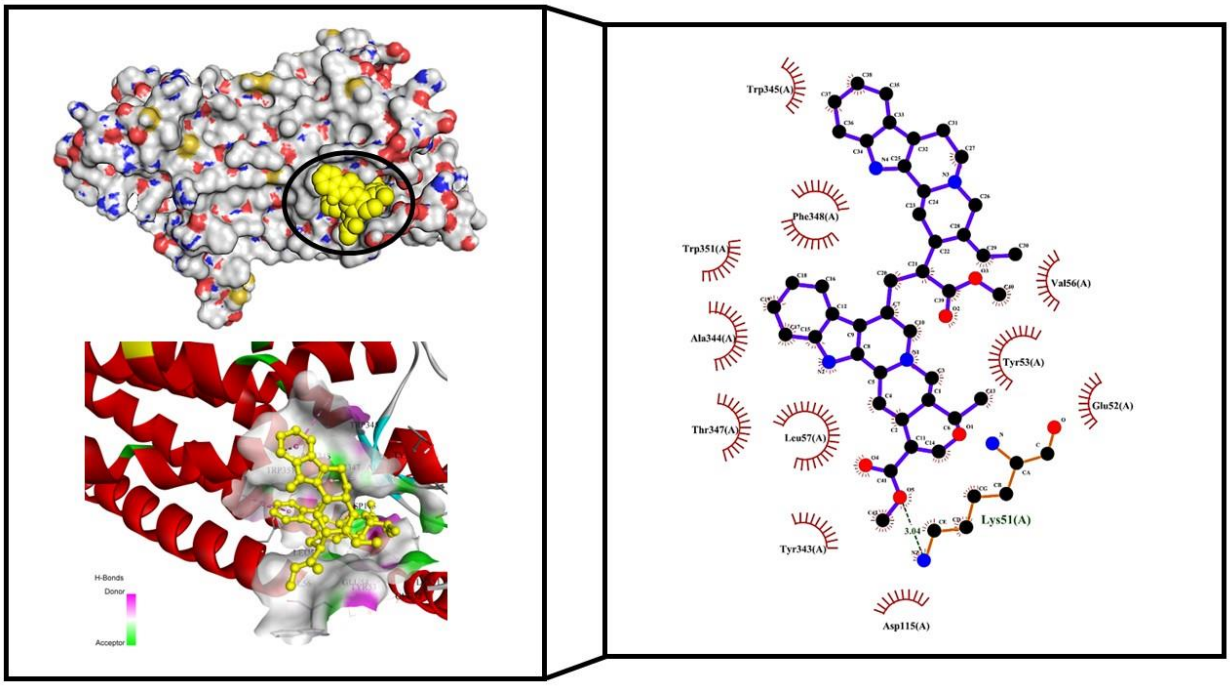
Trp345(A)
Phe348(A)
Trp351(A
Val56(A)
Ala344(A)
Tyr53(A)
Glu52(A)
Thr347(A)
Leu57(A)
Lys51(A)
3.04
Tyr343(A)
Asp115(A)
H-Bonds
Donor
Acceptor

(c)

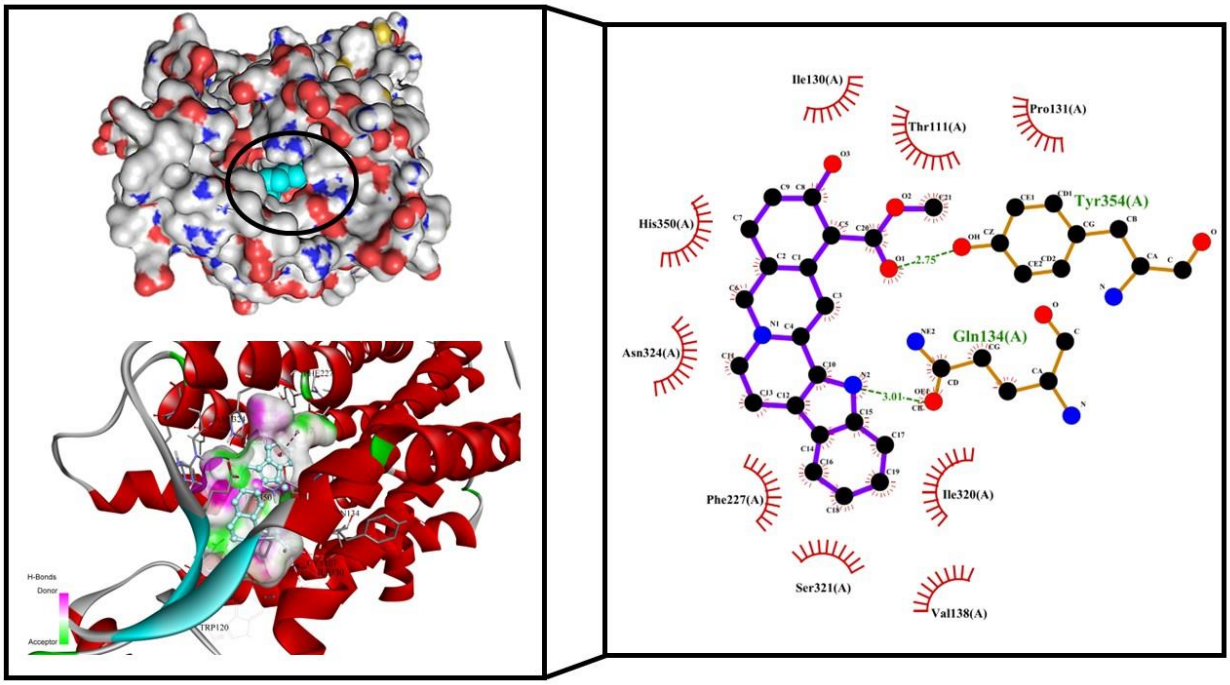

(d)

Figure 10 a-d. Visualization of the interactions between the compounds and the target protein: (a) corynanthine, (b) sarpagine, (c) tetraphyllin, and (d) yohimbine

3. Conclusion

This study focuses on the use of bioinformatic tools to identify novel phytochemicals that could serve as agonists of OX2R receptors for the treatment of narcolepsy. We have employed various computational tools to analyze binding affinity, stability, ADMET properties, drug-likeness properties and protein–ligand interactions to elucidate hit compounds. Various steps, including molecular docking, molecular dynamic simulation, and ADMET analysis, were employed to achieve our goal. On the basis of the results of the aforementioned analysis, we conclude that among the various phytochemicals present in *R. serpentina*, tetraphylline and yohimbine could serve as agonists of OX2R and, subsequently, could be potent drug candidates for the treatment of narcolepsy. However, as this study is purely based on computational or *in silico* findings, thus *in vivo* and *in vitro* studies are needed to further validate their efficacy and potency.

Availability of data and material: The dataset generated or analysed during the study are available from the corresponding author on reasonable request.

References

Chavda, V., Chaurasia, B., Umana, G. E., Tomasi, S. O., Lu, B., & Montemurro, N. (2022). Narcolepsy-A Neuropathological Obscure Sleep Disorder: A Narrative Review of Current Literature. Brain sciences, 12(11), 1473. https://doi.org/10.3390/brainsci12111473

Chin, W. C., Wang, C. H., Huang, Y. S., Hsu, J. F., Chu, K. C., Tang, I., & Paiva, T. (2022). Quality of life changes and their predictors in young adult narcolepsy patients after treatment: A real-world cohort study. Frontiers in psychiatry, 13, 956037. https://doi.org/10.3389/fpsyt.2022.956037

Schokman, A., Cheung, J., Milton, A., Naehrig, D., Thornton, N., Bin, Y. S., Kairaitis, K., & Glozier, N. (2024). Making sense of narcolepsy: A qualitative exploration of how persons with narcolepsy perceive symptoms and their illness experience. Sleep medicine, 116, 62–70. https://doi.org/10.1016/j.sleep.2024.02.026

Pizza, F., Filardi, M., Moresco, M., Antelmi, E., Vandi, S., Neccia, G., Mazzoni, A., & Plazzi, G. (2020). Excessive daytime sleepiness in narcolepsy and central nervous system hypersomnias. Sleep & breathing = Schlaf & Atmung, 24(2), 605–614. https://doi.org/10.1007/s11325-019-01867-7

Alam, M., Abbas, K., Sharf, Y., & Khan, S. (2024). Impacts of blue light exposure from electronic devices on circadian rhythm and sleep disruption in adolescent and young adult students. Chronobiol Med, 6, 10-14. https://doi.org/10.33069/cim.2024.0004

Golden, E. C., & Lipford, M. C. (2018). Narcolepsy: Diagnosis and management. Cleveland Clinic journal of medicine, 85(12), 959–969. https://doi.org/10.3949/ccjm.85a.17086

Latorre, D., Sallusto, F., Bassetti, C. L. A., & Kallweit, U. (2022). Narcolepsy: a model interaction between immune system, nervous system, and sleep-wake regulation. Seminars in immunopathology, 44(5), 611–623. https://doi.org/10.1007/s00281-022-00933-9

Evans, R., Kimura, H., Alexander, R., Davies, C. H., Faessel, H., Hartman, D. S., Ishikawa, T., Ratti, E., Shimizu, K., Suzuki, M., Tanaka, S., Yukitake, H., Dauvilliers, Y., & Mignot, E. (2022). Orexin 2 receptor-selective agonist danavorexton improves narcolepsy phenotype in a mouse model and in human patients. Proceedings of the National Academy of Sciences of the United States of America, 119(35), e2207531119. https://doi.org/10.1073/pnas.2207531119

Andlauer, O., Moore, H., 4th, Hong, S. C., Dauvilliers, Y., Kanbayashi, T., Nishino, S., Han, F., Silber, M. H., Rico, T., Einen, M., Kornum, B. R., Jennum, P., Knudsen, S., Nevsimalova, S., Poli, F., Plazzi, G., & Mignot, E. (2012). Predictors of hypocretin (orexin) deficiency in narcolepsy without cataplexy. Sleep, 35(9), 1247–55F. https://doi.org/10.5665/sleep.2080

Nevárez, N., & de Lecea, L. (2018). Recent advances in understanding the roles of hypocretin/orexin in arousal, affect, and motivation. F1000Research, 7, F1000 Faculty Rev-1421. https://doi.org/10.12688/f1000research.15097.1

Liu, L., Wang, Q., Liu, A., Lan, X., Huang, Y., Zhao, Z., Jie, H., Chen, J., & Zhao, Y. (2019). Physiological Implications of Orexins/Hypocretins on Energy Metabolism and Adipose Tissue Development. ACS omega, 5(1), 547–555. https://doi.org/10.1021/acsomega.9b03106

Abdel-Magid A. F. (2022). Orexin Receptor Agonists as Possible Treatment for Narcolepsy and Idiopathic Hypersomnia. ACS medicinal chemistry letters, 13(9), 1411–1412. https://doi.org/10.1021/acsmedchemlett.2c00358

Soya, S., & Sakurai, T. (2020). Evolution of Orexin Neuropeptide System: Structure and Function. Frontiers in neuroscience, 14, 691. https://doi.org/10.3389/fnins.2020.00691

Hellmann, J., Drabek, M., Yin, J., Gunera, J., Pröll, T., Kraus, F., Langmead, C. J., Hübner, H., Weikert, D., Kolb, P., Rosenbaum, D. M., & Gmeiner, P. (2020). Structure-based development of a subtype-selective orexin 1 receptor antagonist. Proceedings of the National Academy of Sciences of the United States of America, 117(30), 18059–18067. https://doi.org/10.1073/pnas.2002704117

Inutsuka, A., & Yamanaka, A. (2013). The physiological role of orexin/hypocretin neurons in the regulation of sleep/wakefulness and neuroendocrine functions. Frontiers in endocrinology, 4, 18. https://doi.org/10.3389/fendo.2013.00018

Thannickal, T. C., Moore, R. Y., Nienhuis, R., Ramanathan, L., Gulyani, S., Aldrich, M., Cornford, M., & Siegel, J. M. (2000). Reduced number of hypocretin neurons in human narcolepsy. Neuron, 27(3), 469–474. https://doi.org/10.1016/s0896-6273(00)00058-1

Mochizuki, T., Crocker, A., McCormack, S., Yanagisawa, M., Sakurai, T., & Scammell, T. E. (2004). Behavioral state instability in orexin knock-out mice. Journal of Neuroscience, 24(28), 6291-6300. https://doi.org/10.1523/JNEUROSCI.0586-04.2004

Peyron, C., Faraco, J., Rogers, W., Ripley, B., Overeem, S., Charnay, Y., Nevsimalova, S., Aldrich, M., Reynolds, D., Albin, R., Li, R., Hungs, M., Pedrazzoli, M., Padigaru, M., Kucherlapati, M., Fan, J., Maki, R., Lammers, G. J., Bouras, C., Kucherlapati, R., … Mignot, E. (2000). A mutation in a case of early onset narcolepsy and a generalized absence of hypocretin peptides in human narcoleptic brains. Nature medicine, 6(9), 991–997. https://doi.org/10.1038/79690

Yukitake, H., Fujimoto, T., Ishikawa, T., Suzuki, A., Shimizu, Y., Rikimaru, K., Ito, M., Suzuki, M., & Kimura, H. (2019). TAK-925, an orexin 2 receptor-selective agonist, shows robust wake-promoting effects in mice. Pharmacology, biochemistry, and behavior, 187, 172794. https://doi.org/10.1016/j.pbb.2019.172794

Fujiki, N., Yoshida, Y., Ripley, B., Mignot, E., & Nishino, S. (2003). Effects of IV and ICV hypocretin-1 (orexin A) in hypocretin receptor-2 gene mutated narcoleptic dogs and IV hypocretin-1 replacement therapy in a hypocretin-ligand-deficient narcoleptic dog. Sleep, 26(8), 953–959. https://doi.org/10.1093/sleep/26.8.953

Paul, S., Thilagar, S., Nambirajan, G., Elangovan, A., Lakshmanan, D. K., Ravichandran, G., ... & Murugesan, S. (2022). Rauwolfia serpentina: A Potential Plant to Treat Insomnia Disorder. Sleep and Vigilance, 6(1), 31-40. https://doi.org/10.1007/s41782-021-00192-y

Kumar, S., Kumari, D., & Singh, B. (2022). Genus Rauvolfia: A review of its ethnopharmacology, phytochemistry, quality control/quality assurance, pharmacological activities and clinical evidence. Journal of ethnopharmacology, 295, 115327. https://doi.org/10.1016/j.jep.2022.115327

Sofowora, A., Ogunbodede, E., & Onayade, A. (2013). The role and place of medicinal plants in the strategies for disease prevention. African journal of traditional, complementary, and alternative medicines : AJTCAM, 10(5), 210–229. https://doi.org/10.4314/ajtcam.v10i5.2

Vaou, N., Stavropoulou, E., Voidarou, C., Tsigalou, C., & Bezirtzoglou, E. (2021). Towards Advances in Medicinal Plant Antimicrobial Activity: A Review Study on Challenges and Future Perspectives. Microorganisms, 9(10), 2041. https://doi.org/10.3390/microorganisms9102041

Abbas, K., Alam, M., Ansari, M. S., Khan, A., Raza, M. T., Khan, Z., ... & Usmani, N. (2024). Isorauhimbine and Vinburnine as Novel 5-HT2A Receptor Antagonists From Rauwolfia serpentina for the Treatment of Insomnia: An In Silico Investigation. https://doi.org/10.33069/cim.2024.0023

Roy, A., Khan, A., Ahmad, I., Alghamdi, S., Rajab, B. S., Babalghith, A. O., Alshahrani, M. Y., Islam, S., & Islam, M. R. (2022). Flavonoids a Bioactive Compound from Medicinal Plants and Its Therapeutic Applications. BioMed research international, 2022, 5445291. https://doi.org/10.1155/2022/5445291

Shah, S. M. A., Naqvi, S. A. R., Munir, N., Zafar, S., Akram, M., & Nisar, J. (2020). Antihypertensive and Antihyperlipidemic Activity of Aqueous Methanolic Extract of Rauwolfia Serpentina in Albino Rats. Dose-response : a publication of International Hormesis Society, 18(3), 1559325820942077. https://doi.org/10.1177/1559325820942077

Singh, K., Maurya, H., Singh, P., Panda, P., Behera, A. K., Jamal, A., ... & Sharma, D. (2023). DISPEL: database for ascertaining the best medicinal plants to cure human diseases. Database, 2023, baad073. https://doi.org/10.1093/database/baad073

Alam, M., Abbas, K., Raza, M. T., Abedi, S. M. H., Haq, H., & Mustafa, M. (2024). Identification of Aquaporin 3 Inhibitors from Santalum album Phytochemicals for Melanoma treatment: A Computational Study: Targeting Aquaporin 3: Santalum Album in Melanoma Therapy. Iranian Journal of Pharmaceutical Sciences, 20(4), 293-314. https://doi.org/10.22037/ijps.v20i4.44925

Alam, M., Abbas, K., Iram, F., Raza, M. T., Mustafa, M., & Zehra, Z. (2024). Molecular docking and dynamics studies of Withania somnifera derived compounds as GABA-A receptor

modulators for insomnia. Chronobiology in Medicine, 6(2), 77-86. https://doi.org/10.33069/cim.2024.0010

Vivek-Ananth, R. P., Mohanraj, K., Sahoo, A. K., & Samal, A. (2023). IMPPAT 2.0: An Enhanced and Expanded Phytochemical Atlas of Indian Medicinal Plants. ACS omega, 8(9), 8827–8845. https://doi.org/10.1021/acsomega.3c00156

Pettersen, E. F., Goddard, T. D., Huang, C. C., Couch, G. S., Greenblatt, D. M., Meng, E. C., & Ferrin, T. E. (2004). UCSF Chimera--a visualization system for exploratory research and analysis. Journal of computational chemistry, 25(13), 1605–1612. https://doi.org/10.1002/jcc.20084

Alam, M., Abbas, K., Saifi, M. F., Abedi, S. M. H., Hussain, M., & Kausar, S. (2023). Rosehip Phytochemicals: A Computational Approach for Inhibiting Protein Kinase C Delta in Hepatocellular Carcinoma Treatment. J Phytopharmacol, 12(6), 341-357. https://doi.org/ 10.31254/phyto.2023.12601

Trott, O., & Olson, A. J. (2010). AutoDock Vina: improving the speed and accuracy of docking with a new scoring function, efficient optimization, and multithreading. Journal of computational chemistry, 31(2), 455–461. https://doi.org/10.1002/jcc.21334

Dallakyan, S., & Olson, A. J. (2015). Small-molecule library screening by docking with PyRx. Methods in molecular biology (Clifton, N.J.), 1263, 243–250. https://doi.org/10.1007/978-1-4939-2269-7_19

Daina, A., & Zoete, V. (2016). A BOILED-Egg To Predict Gastrointestinal Absorption and Brain Penetration of Small Molecules. ChemMedChem, 11(11), 1117–1121. https://doi.org/10.1002/cmdc.201600182

Myung, Y., de Sá, A. G. C., & Ascher, D. B. (2024). Deep-PK: deep learning for small molecule pharmacokinetic and toxicity prediction. Nucleic acids research, 52(W1), W469–W475. https://doi.org/10.1093/nar/gkae254

Molinspiration Chemoinformatics software, https://www.molinspiration.com

Alam, M., Abbas, K., Dar, G. A., & Ahmed, K. (2024). Nootropic Property of Punica grantum Extract as BDNF4 Stimulant for Treatment of Major Depressive Disorder. International Neuropsychiatric Disease Journal, 21(2), 24-35. https://doi.org/10.9734/indj/2024/v21i2424

Lipinski C. A. (2004). Lead- and drug-like compounds: the rule-of-five revolution. Drug discovery today. Technologies, 1(4), 337–341. https://doi.org/10.1016/j.ddtec.2004.11.007

Jayaram, B., Singh, T., Mukherjee, G., Mathur, A., Shekhar, S., & Shekhar, V. (2012). Sanjeevini: a freely accessible web-server for target directed lead molecule discovery. BMC bioinformatics, 13 Suppl 17(Suppl 17), S7. https://doi.org/10.1186/1471-2105-13-S17-S7

Bjelkmar, P., Larsson, P., Cuendet, M. A., Hess, B., & Lindahl, E. (2010). Implementation of the CHARMM Force Field in GROMACS: Analysis of Protein Stability Effects from Correction Maps, Virtual Interaction Sites, and Water Models. Journal of chemical theory and computation, 6(2), 459–466. https://doi.org/10.1021/ct900549r

Lindorff-Larsen, K., Piana, S., Palmo, K., Maragakis, P., Klepeis, J. L., Dror, R. O., & Shaw, D. E. (2010). Improved side-chain torsion potentials for the Amber ff99SB protein force field. Proteins, 78(8), 1950–1958. https://doi.org/10.1002/prot.22711

Oostenbrink, C., Villa, A., Mark, A. E., & van Gunsteren, W. F. (2004). A biomolecular force field based on the free enthalpy of hydration and solvation: the GROMOS force-field parameter sets 53A5 and 53A6. Journal of computational chemistry, 25(13), 1656–1676. https://doi.org/10.1002/jcc.20090

Lopéz-Blanco, J. R., Garzón, J. I., & Chacón, P. (2011). iMod: multipurpose normal mode analysis in internal coordinates. Bioinformatics, 27(20), 2843-2850. https://doi.org/10.1093/bioinformatics/btr497

Alam, M., Abbas, K., Chaudhary, B., Asif, S., & Balti, A. A. (2024). Computational Analysis of Selected Phytochemicals for their PARP Inhibitory Potential in Cancer. Acta Biochimica Iranica, 2(1), 11-21. https://doi.org/10.18502/abi.v2i1.16243

Laskowski, R. A., & Swindells, M. B. (2011). LigPlot+: multiple ligand-protein interaction diagrams for drug discovery. Journal of chemical information and modeling, 51(10), 2778–2786. https://doi.org/10.1021/ci200227u

Yuan, S., Chan, H. S., & Hu, Z. (2017). Using PyMOL as a platform for computational drug design. Wiley Interdisciplinary Reviews: Computational Molecular Science, 7(2), e1298. https://doi.org/10.1002/wcms.1298